Acta Pharmaceutica Sinica B 2024;14(8):3730–3745

Chinese Pharmaceutical Association
Institute of Materia Medica, Chinese Academy of Medical Sciences

Acta Pharmaceutica Sinica B

www.elsevier.com/locate/apsb
www.sciencedirect.com

ORIGINAL ARTICLE

Remote-controlled dexamethasone-duration on eye-surface with a micelle-magnetic nanoparticulate co-delivery system for dry eye disease

Qinxiang Zheng[a,b,†], Chaoxiang Ge[a,b,†], Kexin Li[a,b,†], Longxin Wang[a], Xiaoyu Xia[a,b], Xiao Liu[a], Rashid Mehmood[d,e], Jianliang Shen[a,c,*], Kaihui Nan[a,*], Wei Chen[a,b,*], Sen Lin[a,*]

[a]*National Engineering Research Center of Ophthalmology and Optometry, Eye Hospital, Wenzhou Medical University, Wenzhou 325027, China*
[b]*National Clinical Research Center for Ocular Diseases, Eye Hospital, Wenzhou Medical University, Wenzhou 325027, China*
[c]*Zhejiang Engineering Research Center for Tissue Repair Materials, Wenzhou Institute, University of Chinese Academy of Sciences, Wenzhou 325000, China*
[d]*School of Chemical Engineering, UNSW Sydney, High Street, Building E10, Kensington, NSW 2052, Australia*
[e]*Adult Cancer Program, Lowy Cancer Research Centre, UNSW Sydney, Corner Botany & High Streets, Kensington, NSW 2052, Australia*

Received 4 January 2024; received in revised form 5 April 2024; accepted 15 April 2024

KEY WORDS

Magnetic nanoparticle;
Micelle;
Dexamethasone;
Eye drop;
Bioavailability;

Abstract Dexamethasone (DEX) is used to treat ocular surface diseases. However, regulating DEX duration in tears while preventing its absorption into the anterior chamber is critical for balancing its therapy effects and the side effects. In this study, a novel magnetic nanoparticle (MNP)-micelle (MC) co-delivery system (MMDS) was developed. The MC moiety in the MMDS served as the carrier for DEX and the MNP part endowed the MMDS with magnetic-responsive properties. To extend its residency, the MMDS was magnetically attracted by an external magnet after instilling, which acted as a

*Corresponding authors.
E-mail addresses: shenjl@wiucas.ac.cn (Jianliang Shen), nankh@wmu.edu.cn (Kaihui Nan), chenweimd@wmu.edu.cn (Wei Chen), lin_sen@wmu.edu.cn (Sen Lin).
[†]These authors made equal contributions to this work.
Peer review under the responsibility of Chinese Pharmaceutical Association and Institute of Materia Medica, Chinese Academy of Medical Sciences.

https://doi.org/10.1016/j.apsb.2024.05.004

Dry eye disease;
Cornea;
Conjunctiva

precorneal drug-depot enabling a sustainable release of DEX in tears. With combination of magnet treatment, the topical instillation of MMDS@DEX significantly prolonged the DEX-retention in tears and increased the DEX-concentration in the cornea and conjunctiva, as well as concurrently reduced the DEX-level in the aqueous humor, when compared with the commercial DEX eye drop treatment. The combination of MMDS@DEX and magnet treatment exerted significantly better therapeutic effects against DED with smaller side effects than conventional treatments including DEX suspension, commercial DEX eye drops, as well as the MMDS@DEX treatment alone. The present work provided a new method for the effective delivery of DEX to ocular surface tissues while reducing its side effects, which will be beneficial to the treatments of a wide range of ocular surface diseases.

1. Introduction

Dry eye disease (DED), a multifactorial disease with tear hyperosmosis and persistent ocular surface inflammation, is identified as a localized autoimmune disease characterized by the loss of homeostasis of immune regulation[1,2]. Under DED conditions, the hyperosmotic tear upregulates the pro-inflammatory cytokine in the cornea and conjunctiva, which activates the antigen-presenting cells (APCs) and thus results in the activation of $CD4^+$ T cells. The $CD4^+$ T cells migrate towards the cornea and conjunctiva to evoke the inflammatory cascade reaction, thus causing the losses of corneal epithelium and conjunctival goblet cells[3,4]. Our recent findings have demonstrated that the NLRP3/Caspase-1/GSDMD mediated corneal epithelium pyroptosis is involved in DED-induced corneal epithelium loss[5,6]. NLRP3 (nucleotide-binding domain, leucine-rich-containing family, pyrin domain-containing-3) has the ability to sense and detect a range of stimuli including irritants, microbes, and danger signals. The interaction of these stimuli with NLRP3 causes the formation and activation of NLRP3 inflammasome, which results in the release of pro-inflammatory cytokines IL-1 and IL-18 in a caspase 1-dependent manner as well as the occurrence of gasdermin D-mediated pyroptotic cell death[7]. In view of these facts, it has been reported that a range of inhibitors have been developed to inhibit NLRP3 inflammasome such as dexamethasone (DEX)[8-10].

DEX acts in anti-inflammatory fashion by inhibiting the aggregation of inflammatory cells as well as attenuating the expression of inflammatory cytokines in the matrix[11]. In addition, it inhibits immune responses by suppressing cell mediated immune reactions and preventing delayed-type hypersensitivity (DTH) reactions[12,13]. DEX is one of the most commonly prescribed drugs in ophthalmological clinics for treating inflammation-related eye conditions such as allergies, shingles, iritis, uveitis, injury, infection, *etc*. It works by relieving symptoms such as swelling, redness, and itching. However, repeated instillation of DEX will lead to escalating in intraocular pressure (IOP) after being absorbed into anterior chamber, which are generally considered as its major side effect[14,15]. Therefore, strategies for increasing lacrimal DEX concentration while preventing its absorption into anterior chamber are especially important to balance its therapy effects and side effects, while DEX is topically administrated to treat ocular surface diseases (*e.g*., DED).

Considering the potential of DEX, several types of DEX eye drops are formulated and commercially available for varying eye-related conditions. However, one of the critical drawbacks of the existing DEX formulations is that their low bioavailability requires the need for frequent addition, which causes off-target toxicity issues. The sealed anatomical structure of eyes as well as the rapid tear renewal which can rapidly eliminate the drug from eye surface are the key barriers to effective drug delivery in ocular surface medication[16,17]. Due to its hydrophobic nature, DEX is insoluble in tears (appears as a turbid suspension), which makes it easily to be removed away from eye surface after topical administration. DEX implants such as Dextenza® and Ozurdex® can bypass these onsite barriers because they were developed as the DEX-depot, having the ability for localized sustainable release of DEX, which remarkably increased the DEX-bioavailability and achieved long lasting effects with one time treatment[18,19]. However, as an intravitreal implant, Ozurdex® is not suitable for treating ocular surface diseases. Dextenza® is an intracanalicular insert which can be implanted in the lower lacrimal punctum to treat allergic conjunctivitis. It is limited as the operation and handling procedure require a skilled doctor (or someone who is professionally trained). On the other hand, several nano/microparticles including microspheres, liposomes, nano-capsules, and nano-somes were developed to enhance the *in vivo* bioavailability of drugs and simultaneously reduce their side effects after systemic or topical administration[20-24]. Among such nano-strategies, amphipathic co-polymers-based systems can encapsulate DEX by hydrophobic interaction forming nano-scaled formula, which could enhance DEX's ability for resistance to the onsite barriers on eye surface[5,16,24]. We recently developed a positive charged nano micelle with HKHKHK (peptide) modification, which significantly prolonged the retention of the hydrophobic agents on eye surface[16]. However, these strategies also enhanced *trans*-corneal transporting of the cargo[16,25,26], and thus could increase side effects as well.

Since prolonging drug retention on eye surface concurrently reduces its intraocular transportation, in the present work, we developed a new micelle (MC)-magnetic nanoparticle (MNP) conjugated co-delivery system (MMDS, Fig. 1). The MC was chemically conjugated with the MNP by Michael addition reaction. The MC moiety in the MMDS serves as the carrier for hydrophobic molecules, while the MNP part endows the MMDS with magnetic responsive properties. After instillation, the drug (in the MMDS) on eye surface can be tracked and remote-controlled by external magnet, which enhances its ability for resistance of tear scour, thus endowing it with long residency on eye surface and concomitantly reducing it to be absorbed into the anterior chamber. Theoretically, the retention of the drug (in

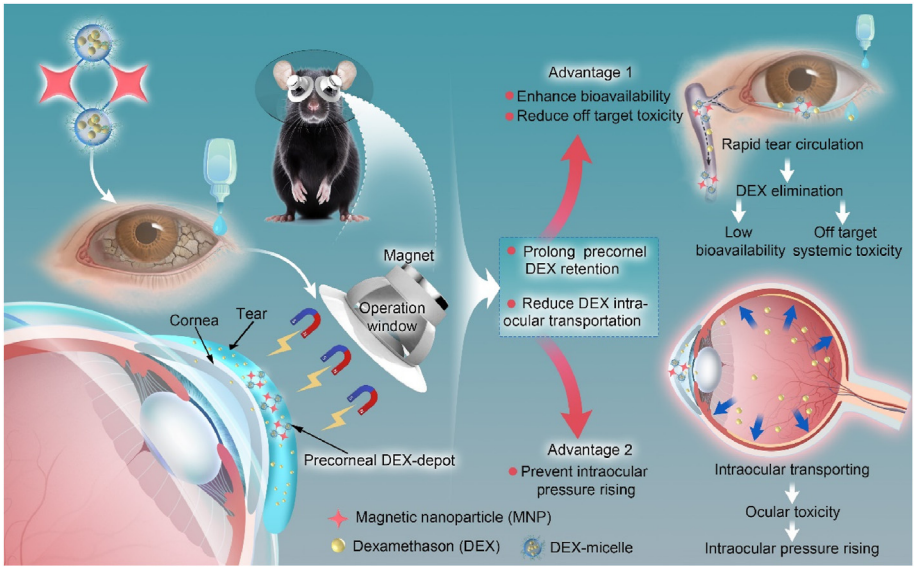

Figure 1 An illustration of the engineering dexamethasone (DEX)-micelle and magnetic nanoparticle (MNP) co-delivery system (MMDS@DEX) as a precorneal DEX-depot for effectively DEX-delivery towards eye-surface tissues to balance its therapy effects and the side effects.

the MMDS) can be easily remote-controlled by regulating the intensity of the external magnetic field. With attraction by external magnet, the MMDS (MMDS+MA) can act as the onsite precorneal drug depot for sustainable release of ophthalmic hydrophobic agents (*e.g.*, DEX, FK506, fluorometholone), which can significantly enhance their bioavailability. Since the low bioavailability is the major limitation of commercial eye drops, the present work provided a new method for the effective delivery of hydrophobic agents to ocular surface tissues while avoiding their side effects, which will be beneficial to the treatments of a wide range of eye surface diseases.

2. Materials and methods

2.1. Chemicals and materials

The AR grade chemicals for MNP preparation and modification including sodium acetate trihydrate (14.4 g), $MgCl_26H_2O$, $FeCl_36H_2O$, and methacrylic acid purchased from Sigma−Aldrich. A new peptide modified micelle (PEP-MC) was employed in this study. The sequence of the peptide, obtained from GL Biochem (Shanghai) Ltd., is HKHKHK. The materials and process for the PEP-MC preparation were consistence with our previously report[16]. Nile red and DEX were purchased from J&K Chemicals Co. (Beijing, China). The human cornea epithelial cells (HCECs) were original from ATCC (Manassas, VA, USA). The chemicals and materials for cell culturing including DMEM-F12 liquid, fetal bovine serum, and insulin were supplied by Gibco (City, CA, USA). Cell counting kit-8 (CCK8) for cell viability assessment was supplied by Dojindo Laboratories (Kumamoto, Japan).

2.2. Preparation and modification of MNPs

The iron based MNPs were prepared using solvent-thermal method[27] with some modifications. Briefly, 7.2 g of sodium acetate trihydrate (14.4 g), 1.02 g of $MgCl_26H_2O$ (2.04 g) and 2.7 g of $FeCl_3$ $6H_2O$ (5.4 g) were mixed in 160 mL of ethylene glycol. The mixture was then transferred to a 500 mL round bottom flask. It was refluxed under 180 °C overnight under vigorously stirring. After cooling, the resultant MNPs were harvested by magnetic decantation. The MNPs were washed with water (3 times) and ethanol (3 times) to remove contaminants. After magnetic decantation, the obtained MNPs were dried in a vacuum oven at 60 °C, and 1.5 g of MNPs were harvested. To obtain the MNP with double bond on its surface, they were further modified with methacrylic acid (MMA). The MNPs (40 mg) were re-suspended in an aqueous solution containing varied amounts of MMA. The mixture was incubated in a constant temperature shaker for 48 h at a shaking rate of 100 rpm. The MMA was attached onto MNPs by the interaction of COOH in the MMA and the hydroxyl groups on the surface of MNPs[28,29]. The MMA modified MNPs (mMNPs) were harvested by magnetic decantation. The attachments of MMA onto the MNPs were analyzed using thermogravimetric (TGA) and inductively coupled plasma mass spectrometer (ICP−MS). Theirs hydrodynamic size, PDI, zeta potential, as well as their stability in the aqueous solution were determined using Malvern ZS-90 dynamic light scattering laser particle size analyzer (DLS).

2.3. Preparation and characterization of the MMDS

The PEP-MC was prepared and characterized in our previous report[16]. The sequence of HKHKHK was applied which endows the enrichment of PEP-MC in the primary amino group on its surface. The PEP-MC was conjugated to mMNPs using Michael addition reaction. Briefly, the PEP-PGE-PBG based MC was mixed with mMNPs in sodium hydroxide solution and incubated in room temperature overnight for sufficient reaction. The MMDS was harvested using magnetic decantation. The conjugation rate of mMNPs onto the MC was determined TGA and ICP-MS. The morphologies of MMDS were observed by transmission electron microscopy (TEM, Tecnai G2 F20 S-TWIN, FEI).

2.4. Encapsulations and release of DEX

For the encapsulation of DEX, varied amounts of DEX was mixed with 1 mg of MMDS in DMF (1 mL). After adding excessive

distilled water drop-wise under stirring, DEX was entrapped into the hydrophobic core of the MMDS by hydrophobic interaction. The DEX entrapped MMDS (MMDS@DEX) was harvested by magnetic decantation. After freeze-drying, the MMDS@DEX was weighted and redissolved in DMF to release the entrapped DEX. After magnetic decantation, the supernatant (containing the released DEX) was obtained, and subsequently diluted with methanol. The DEX was quantitatively analyzed using a UPLC (Shimadzu LC-8050) coupled with tandem MS with an electrospray ionizer (ESI) and a triple quadrupole mass analyzer, separated by an Shim-pack XR-ODSIII column (2.0 mm id × 50 mm, particle size: 1.6 μm). After appropriate dilution, 2 μL of the sample was loaded onto the column, and eluted by 0.1% formic acid (in distilled water, A phase) and acetonitrile (B phase) at a speed of 0.4 mL/min with the following gradient process: 0−4.5 min, 20%−90% B; 6 min, 90% B; 7 min, 20% B; 9 min, 20% B. The targets were monitored under multiple reactions monitoring (MRM) mode in positive ionization mode with a capillary voltage of 4 kV. The gas flow rates for nebulizing, drying, and heating were fixed at 3, 10 and 10 L/min, respectively. The temperature of the interface, desolvation area, and heart block were set at 400, 150, and 450 °C, respectively. The integral peak area of the ion with m/z 393.4 > 355.1 was adopted for the quantification. The encapsulation rate (ER) of DEX was expressed as the percentage of the encapsulated DEX in MMDS@DEX.

The *in vitro* release profiles of DEX from the MC and MMDS were determined using the method described previously[16], with minor modifications. Briefly, 1 mL of varied DEX formulas (DEX in the MC, DEX in the MMDS, or DEX suspension) containing 0.2 mg of DEX were embedded into dialysis bags with a molecule weight cut off 3500 Da. They were then dialyzed against 30 mL of distilled water under 37 °C at a shaking rate of 150 rpm. At regular time intervals, 2 mL of the dialysate was replaced with fresh water. The DEX in dialysate was quantitatively analyzed by UPLC−MS-MS using the above-mentioned method.

To visualize the magnetic responsive properties of the MMDS, the Nile red (fluorescence probe) instead of DEX was loaded into the MMDS. The suspension of Nile red encapsulated MMDS (MMDS@NR) was then treated by a magnet. The behaviors of MMDS@NR under external magnetic field were recorded by a digital camera. To further quantify its magnetic responsive properties, the Nile red encapsulated MC (MC@NR) was reacted with varied amounts of mMNPs producing varied MMDS@NRs containing different amounts of mMNPs. The MMDS@NRs (with different mMNP contents) were harvested using magnetic decantation, while the un-reacted MC@NR presenting supernatants were discarded. After washing twice with fresh water, the MMDS@NRs were resuspended in DMF to release the encapsulated Nile red. After being appropriately diluted, the Nile red in DMF was then quantified by measuring the fluorescence intensity (excitation at 543 nm; emission at 598 nm).

2.5. *The in vitro and in vivo toxicity evaluation*

The cytotoxicity of MNPs, mMNPs, and the MMDS against HCEC were evaluated using the CCK-8 assay[6]. Briefly, the HCEC was maintained in DMEM-F12 (Gibco) medium supplemented with FBS (10%, *v/v*, Gibco), insulin (5 μg/mL), and epidermal growth factor (10 ng/mL). An aqueous solution of HCEC was seeded in a 96-well plate at a density of 5000 cells per well. The 96-well plates were kept in an incubator under 37 °C with atmospheric conditions of 5% CO_2 and 90% humidity. To evaluate the cytotoxicity, the HCEC was co-cultured with different amounts of MNPs, mMNPs, and the MMDS for 24 and 48 h, respectively. The cell was then cultured for 2 h in the medium containing 10% (*v/v*) of the CCK-8 liquid. The absorbance at 450 nm was recorded. Cell survival rate was calculated as the percentage of absorbance from treated cells to that of untreated control cells. The *in vivo* cumulative toxicity of the MMDS was evaluated by continuously dropping of MMDS suspension (15 μL, 7.8 mg/mL) into the conjunctival sac of healthy C57BL/6 mice (age: 6−8 weeks, weight: 18−22 g) for 5 days at a frequency of 3 times a day. The *in vivo* safeties of the MMDS with presence and absence of external magnet treatment were compared. The corneas of the animals underwent general ophthalmological examination by a slit lamp after fluorescein sodium staining[16,17], in which all the factors harmful to corneas were recorded as green dots. The sections of the corneas from the animals receiving varied treatments were prepared and H&E-stained. Any histological changes in the cornea were recorded by a microscope. Excess iron deposition in the cornea and conjunctiva can be toxic to these tissues by generating oxygen free radicals through the Fenton reaction[30]. The content of Fe in the cornea and conjunctiva respectively was determined using ICP-MS after continuous MMDS exposure. The situations with and without external magnet presence were compared.

DEX leads to an increase intra-ocular pressure (IOP) which is recognized as the major side effects when applied to ocular surface. The *in vivo* changes in IOP were measured on healthy animals after reviewing following treatments: 1) MMDS@DEX with magnetic attraction (MMDS@DEX+MA); 2) MMDS@DEX without magnetic attraction (MMDS@DEX); 3) commercial DEX eye drops; 4) DEX suspension; 5) without any treatment. The animals were continuously instilled with 30 μL of DEX formula (DEX concentration: 0.2 mg/mL) for 12 days at a frequency of 5 times/day. Their IOPs were measured 2 h after DEX administration.

In vivo assessment of the effects of external magnetic field on the MMDS@DEX distribution: to understand whether the distribution of DEX can be remotely controlled by external magnetic field, the DEX-MMDS instillations with or without magnet treatment were conducted; and the concentrations of DEX in tears, corneas, conjunctivas, and the aqueous humor were determined in time course after administration. To evaluate the DEX retention in tears, 30 μL of MMDS@DEX (containing 0.2 mg/mL of DEX) was instilled into the conjunctival sac of rabbits. At designated time interval, tears were sampled by emerging filter paper (1×1 cm) into tears for 5 s[16]. The DEX was extracted from the filter papers by soaking the sampling paper in 1 mL of methanol for 10 min under ultrasound treatment[16]. After appropriate dilution, the DEX was quantitatively analyzed by UPLC coupled with tandem MS using the above-mentioned method. At 0.5, 2, 4, and 8 h of treatments, the animals were sacrificed, and their corneas and conjunctivas were extracted. The obtained tissues (corneas or conjunctivas) were scraped into cyclic shape with a trephine (5 mm in diameter). They were then finely grounded in a solvent of methanol/acetonitrile (8/2, *v/v*) to release the DEX. The resultant samples were then subjected to ethyl acetate extraction. After removing ethyl acetate by nitrogen flow, the samples were re-dissolved in methanol, and the amount of DEX in each piece of tissues ($\approx$19.625 mm^2) was determined. The corneal permeability of MMDS@DEX with or without magnet treatment was assessed by measuring the DEX concentration in the aqueous humor at 15, 30, 60, 120, 240 min after administration.

2.6. *In vivo therapy effects against DED*

The C57BL/6 mice (age: 6−8 weeks, weight: 18−22 g) were obtained from Shanghai Jiesijie Experimental Animal Co., Ltd. (Shanghai, China). They were maintained in the Experimental Animal Center of Wenzhou Medical University (WMU). For DED-modeling, the mice were kept in an air-conditional oven with environmental conditions of 21−23 °C in temperature, 13.1 ± 3.5% in humidity, and 2.1 ± 0.2 m/s in air flow[17]. The experiments were conducted with following groups (treatments): 1) DED animals with MMDS@DEX instillation and magnet attraction; 2) DED animals with MMDS@DEX instillation; 3) DED animals with commercial DEX eye drop instillation; 4) DED animals with DEX suspension instillation; 5) DED animals with PBS instillation; and 6) healthy animals with PBS instillation. The animals were continuously treated with 15 μL of DEX formula (0.2 mg/mL) at a frequency of 3 times/day. The animals were medically examined by a skilled doctor using a slit lamp microscopy according to the previous method[16]. After staining with 2% fluorescein, the corneas were observed under slit lamps. All the defections in the cornea were fluorescein-stained and thus exhibited as green signal under slit lamps. The progress of DED can be graded by the profile of cornea fluorescein staining according to the criteria provided by the National Eye Institute (USA). Specifically, the cornea was separated into the central-, bitemporal side-, nasal side-, upward-, and downward-regions. The staining spots in each region were evaluated and scored by a skilled doctor according to the standard of marking no obvious staining as "0", and the spread-, diffused-, and agglomerate-staining as "1", "2", and "3", respectively. The total score for each animal was the sum of the score of each region. The animal experiments were reviewed and approved by the Ethical Review Committee for Experimental Animals in Wenzhou Medical University.

2.7. *qPCR assay*

The mRNA was extracted using RNeasy Mini Kit (QIAGEN, Crawley, UK). After sacrificing the animals, the tissues were extracted and cut into small pieces. To release the mRNA, the tissues were disrupted in the buffer RLT (500 μL, RLT: β-mercaptoethanol = 100:1), and then mixed with 70% ethanol solution (500 μL). After loading onto the RNeasy Mini spin column, the mRNA was obtained by eluting this column following the process provided by the manufactory. After reverse-transcribing the obtained mRNA to complementary DNAs (cDNAs), qPCR was operated on a realtime PCR machine (CFX96, Bio-Rad, USA) employing the Platinum SYBR Green qPCR SuperMix-UDG (Invitrogen, Carlsbad, CA, USA). The primer sequence for target genes was listed in Supporting Information Table S1. The expression of GAPDH which serves as an internal control was tested concurrently. The mRNA expression levels of target genes were calculated by comparing their threshold cycle of target genes and the internal control (GAPDH). Each treatment was conducted with 3 times of biological duplication. Each sample was performed with 3 times of the parallel PCR amplification.

2.8. *Enzyme-linked immune sorbent assay (ELISA)*

The eye surface tissues from the experimental animals were extracted and cut into small patches. The tissue patches were merged in the tissue lysis buffer and grounded for 10 min and sequence lysis for another 2 h (operated under ice bath). The contents of crude proteins in the lysates were quantitatively analyzed using Pierce™ BCA Protein Assay Kit following the process provided by the manuscript. After appropriate dilution, the contents of IL-1β and TNF-α in tissues after receiving varied treatments were measured using ELISA kit (abs520001 and abs520010, Absin, Shanghai, China) according to the manufacturer's instructions.

2.9. *Histochemical examinations*

The eyeballs of the animals receiving varied treatments were enucleated and fixed in 4% paraformaldehyde overnight. After embedded in paraffin, the sections with a thickness of 5 μm were prepared. To evaluate the protective effects on conjunctiva goblet cells, the conjunctiva section originated from animals receiving varied treatments were stained and examined using Glycogen Periodic Acid Schiff (PAS/Hematoxylin) Stain Kit (G1281, Solarbio Co., Shanghai, China) according to the manufacturer's instructions. The morphologies of goblet cells in conjunctivas were recorded by a Nikon digital camera at 20× magnification. The TUNEL assay was then adopted to evaluate the protective effects of these treatment on corneas using previously reported method[31].

2.10. *Statistical analysis*

Statistical analyses were conducted, and one/two-way analysis of variance (ANOVA) was adopted to examine all the significant differences existed in the outcomes of varied treatments at confidence levels of 95% ($*P < 0.05$), 99% ($**P < 0.01$), and 99.9% ($***P < 0.001$).

3. Results and discussion

3.1. *Preparation and characterization of MNPs and mMNPs*

The synthesis process for MMDS preparation is shown in Fig. 2A. The MNPs were obtained by the reaction of $FeCl_3 6H_2O$, $MgCl_2 6H_2O$ and sodium acetate trihydrate in thermos-solvent (180 °C), and were further modified with methacrylic acid (MMA), resulting in MMA grafted MNPs (mMNPs). To prepare the MMDS, the double bond of MMA-MNPs was coupled with the MMDS and was formed by the coupling of mMNPs and MMA grafted MNPs (mMNPs) from the amino groups on the surface of the peptide modified MC (preparation and characterization of the peptide modified MC present in our previous report[16]) in an alkaline solution. The phase structures of MNPs and mMNPs were determined using X-ray diffraction (XRD, Fig. 2B). Peaks at 2-theta degree (2-θ) of 21.5°, 35.2°, 41.5°, 50.6°, 63.2°, 67.5°, and 74.4° are consistent and corresponding with PDF#73-2211 data for Fe_2MgO_4 nanoparticles described in previous reports[32,33]. Modification of MNPs with MMA does not cause significant impact on its characteristics of phase structures. To understand the chemical state of iron in MNPs and mMNPs, samples were subjected to X-ray photoelectron spectroscopy (XPS) analysis, where survey scanning of MNPs and mMNPs suggested that they contain the elements of Fe, O, Mg, and C (Supporting Information Fig. S1). The high-resolution scanning spectra at the binding energy range of 700−740 eV appeared two-character peaks at 710.7 eV (accompanied with a satellite peak at 719.4 eV) and 724.4 eV (accompanied with a satellite peak at 733.7 eV) (Fig. 2C) are corresponding to the Fe 2p 3/2 and Fe2p 1/2 of Fe_2O_3[34-36], respectively. The high-resolution scanning spectra for O1s of MNPs is present in Fig. 2D. As depicted, the O1s spectrum

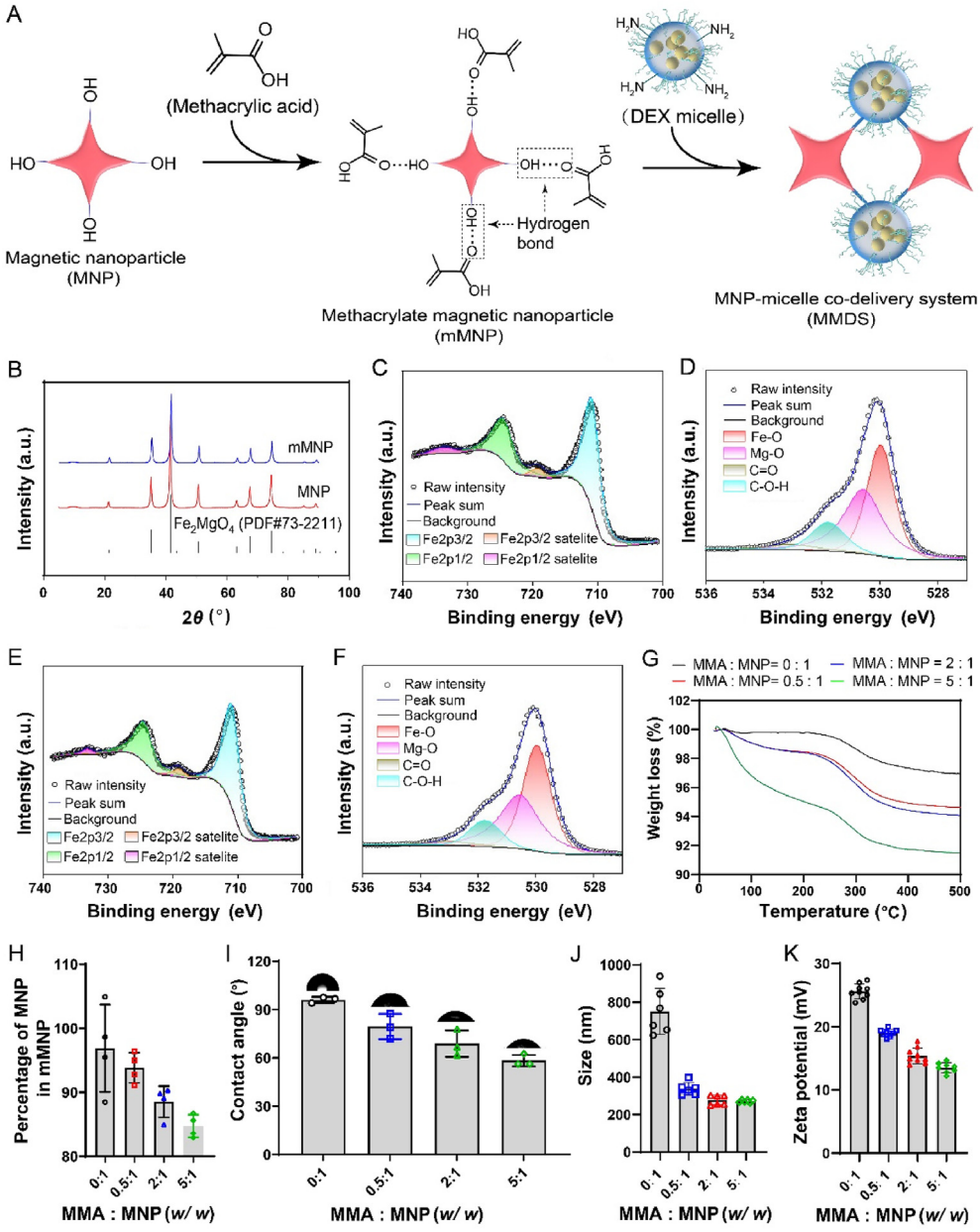

Figure 2 Characterization of the MNP and mMNP. (A) Schematic illustration of the process for MNP modification and MMDS preparation. (B) XRD patterns of the MNP and mMNP. (C) and (D) High-resolution XPS spectra of the MNP with peaks fitting Fe (Fe 2p3/2 and Fe2p1/2) and O (O1s). (E) and (F) High-resolution XPS spectra of the mMNP with peaks fitting Fe (Fe 2p3/2 and Fe2p1/2) and O (O1s). (G) TGA diagrams of the MNP with modification by varied amounts of methacrylic acid. (H) Attachments of the MMA onto MNP (measured by ICP-MS). Data are expressed in mean ± SD ($n = 4$). (I) Changes in the wettability of the mMNP with grafting varied amounts of MMA. Data are expressed in mean ± SD ($n = 3$). (J) and (K) Changes in the size and zetapotential of the mMNP, respectively, with grafting varied amounts of MMA. Data are expressed in mean ± SD ($n \geq 5$).

has a typical peak at the binding energy of 530.08 eV, indicating the existence of metal oxide[37]. The peak for O1s in spectrum of MNPs could resolve into peaks including Fe−O lattice oxygen (529.9 eV)[34], Mg−O lattice oxygen (530.5 eV)[38], and surface hydroxyl (C−OH, 531.7 eV)[34]. No obvious difference in XPS spectra can be observed between MNPs and mMNPs (Fig. 2E and F and S1B), suggesting MNPs with MMA does not significantly impact chemical states of Fe and Mg in the magnetic nanoparticle.

The MMA was attached onto the surface of MNPs with hydrogen bond interaction between the carboxyl group (in MMA) and the hydroxyl group (on the surface of MNPs). After mixing with varied amounts of MMA, the amount of MMA attached onto the surface of MNPs was determined by thermogravimetric analysis (TGA) and the inductively coupled plasma mass spectrometry (ICP−MS). As shown in Fig. 2G, there are no obvious mass loss at the operating temperature of <180 °C, suggesting there are no water (free and combined) existed on the surface of MNPs. Slight weight loss (less than 1% of mass losses) was observed at the temperature range of 185−500 °C, probably due to the minor glycol (boiling point 197.30, applied as the solvent for

MNP preparation) contamination on the surface of MNPs. After modification with MMA, the mMNPs exhibited two distinct weight loss steps in the temperature range of 30−500 °C, where the first weight loss (30−180 °C) is mainly contributed by the removal of the water on the surface of nanoparticles, while the second weight loss (200−400 °C) is attributed to the loss of MMA. The amounts of MMA in mMNPs were quantitatively analyzed by ICP−MS using pristine MNPs as the standard. With the increase in the feeding ratio of MMA/MNP, the MMA on the surface of MNPs was increased (Fig. 2H). It reached 12% of the total mMNP amount, when feeding ratio of 5/1 (MMA/MNP, *w*/*w*) were applied (Fig. 2H). Moreover, changes in wettability of nanoparticle modification with MMA were observed. After modification with MMA, the contact angles dramatically dropped from 92 (bare MNPs) to 60 (feeding ratio of MMA/MNP = 1:5) (Fig. 2I), indicating the increase in wettability after modification. These results explain the obvious weight loss (loss of surface water) in the temperature range of 30−180 °C in the TGA assessment of mMNPs (Fig. 2G). The changes in hydrodynamic size, zeta potential, and PDI were assessed by a Marven ZS-90 dynamic light scattering (DLS). The pristine MNPs exhibited as aggregated heterogeneous particles with a hydration size varying from 600 to 1000 nm (Fig. 2J) and PDIs>0.5 (Supporting Information Fig. S2). Significant drop of the particle sizes as well as the PDIs were observed after attachments of MMA onto MNPs. Nanoparticles with a hydration size around 260 nm and PDI of 0.18 were achieved, when feeding ratio of 5/1 (MMA/MNP, *w*/*w*) was applied (Fig. 2J and S2). The zeta potentials decreased from 25 to 15 mV with the increase of the feeding ratio of MMA/MNP from 0/1 to 5/1 (Fig. 1K), which further confirmed the attachment of MMA onto MNPs.

The stability of MNPs and mMNPs were assessed by monitoring the changes in size, PDI, and count rate in time course using DLS. As shown in Supporting Information Fig. S3A, pristine MNPs were unstable and aggregatively sinking to the bottom of the bottle in 2 h at which time point most of mMNPs are suspended in the aqueous solution. Moreover, a large part of mMNPs is remain suspended in the aqueous solution even with the static cultured for 1 day, which indicated obviously improvement in the stability of the nanoparticles in the aqueous solution after modification of MMA. Dramatically changes in hydration size, PDI, and count rate of bare MNPs were observed during the monitoring time range (Fig. S3B−D), while their changes maintained at certain values for mMNPs, which further indicated the enhanced stability of these nanoparticles after MMA medication. These results were consistent with the observation shown in Fig. S3A. Additionally, it is evident that increasing the feeding amount of MMA from 0.5/1 to 5/1 does not likely further improve its stability.

3.2. *Preparation and characterization of the MMDS*

The mMNPs were chemically conjugated with peptide (HKHKHK) modified micelle (PEP-MC) by Michael addition reaction through C=C double bond of mMNPs and amino groups in the PEP-MC under alkaline conditions. The resultant product was harvested using magnetic attraction. The conjugation rates of the micelle onto mMNPs were determined by measuring the mMNP contents in the MMDS using ICP-MS technique. As shown in Supporting Information Fig. S4, the increase of the alkaline concentration from 0.5 mmol/L to 1 mmol/L significantly improved the reaction between the C=C double bond and amino groups, which increased the ratio of micelle in the MMDS from 11% to 45%. However, further increase in the alkaline concentration did not facilitate the further conjugation of mMNPs and PEP-MC. The chemical structure of MMDS was investigated using Fourier transform infrared spectroscopy (FT−IR) and Raman spectroscopy techniques. The FT−IR spectra of HKHKHK modified PEG-PBG has shown primary amine N−H stretching vibration (symmetrical $\nu_{N-H,\ s}$; and asymmetrical, ν_{N-H}, as) at 3296 cm^{-1}, the characteristic C−H bending vibration (δ_{C-H}) peaks for mono-substituted aromatic ring at δ_{C-H} 744 and 696 cm^{-1}, as well as the amide I, II, and III band at 1650, 1545 and 1240 cm^{-1} (Supporting Information Fig. S5A), respectively, which are consistence with our previous report[15]. The FT−IR spectra of MNPs exhibited an O−H stretching and bending vibration band at 3412 and 1652 cm^{-1}, respectively (Fig. 3A)[39]. The characteristic Fe−O stretching and bending vibration peaks were observed at 548 and 435 cm^{-1}, respectively[39,40]. The peaks at 1728, 1425, and 1370 cm^{-1} in the FT−IR spectra of mMNPs were attributed to the stretching vibration of C=O (in the carboxyl group), and C−H stretching vibration in CH_3, which further confirmed the successful attachment of MMA onto MNPs. Furthermore, the peaks at 3447, 1731, 1586, 1354, and 1241 cm^{-1} (contributed by PEP-PEG-PBG), as well as the characteristic Fe−O stretching and bending vibration peaks at 545 and 436 cm^{-1} can be observed in the FT−IR of MMDS, indicating the obtainment of the MNP and MC conjugated co-delivery system. These results can be further confirmed by Raman spectra (Fig. 3B and Fig. S5). The amounts of PEP-PEG-PBG grafted onto MNPs were evaluated by TG and ICP−MS. As shown in Fig. 3C, increasing the feeding ratio of MNP/MC, the amounts of MC in the harvested MMDS (by magnetic attraction) were increased from 10% to 35%, which can be further confirmed by the results of TG (Fig. 3D). The wettability of the MMDS was enhanced with the increase in the content of MC in the MMDS (Fig. 3E). The MMDS has hydration sizes around 500−700 nm with PDIs of 0.3−0.4 (Fig. 3F and G). The mMNPs are positively charged with nanoparticles with a zeta potential of 15 mV (Fig. 3H). After conjugation with the micelle, the zeta potentials of mMNP-MC (MMDS) became negatively charged with a zeta potential varying from −10 to −20 mV (Fig. 3H). The stability of MMDS in the aqueous solutions was evaluated by tracing the changes in the hydration size, PDI, and zeta potential by DLS. As depicted in Fig. 3I and Supporting Information Fig. S6, the resultant MMDS produced by feeding ratio of mMNP:MC = 1:1 of the conjugation reaction (with the MC content less than 10%) is unstable and aggregatively forms large particles within several minutes. The morphologies of MMDS, mMNPs, and MNPs were observed by TEM. As shown in Fig. 4A and B, the MNP spherical nanoparticle mainly composed by Fe and O elements. The TEM images of MMDS possessed high contrast (attributed to MNPs) areas and low contrast areas (attributed to MC) (Fig. 4C and D, Supporting Information Figs. S7 and S8). The Fe-element was distributed on the MNPs moiety (high contrast areas, exhibited as several separated particles) of MMDS (Fig. 4C and S8). While the C- and N-elements which mainly contributed by the MC moiety were eventually distributed in both the high contrast and low contrast areas (Fig. 4C and S8). These results suggested that several separated MNPs (high contrast under TEM) were connected by MC (low contrast under TEM), thus forming MNP and MC conjugated nano/micro-structures. Furthermore, the high-resolution TEM (HRTEM) images of MMDS reveal a regularly crystal system with obvious lattice fringes at a distance of 0.35 nm

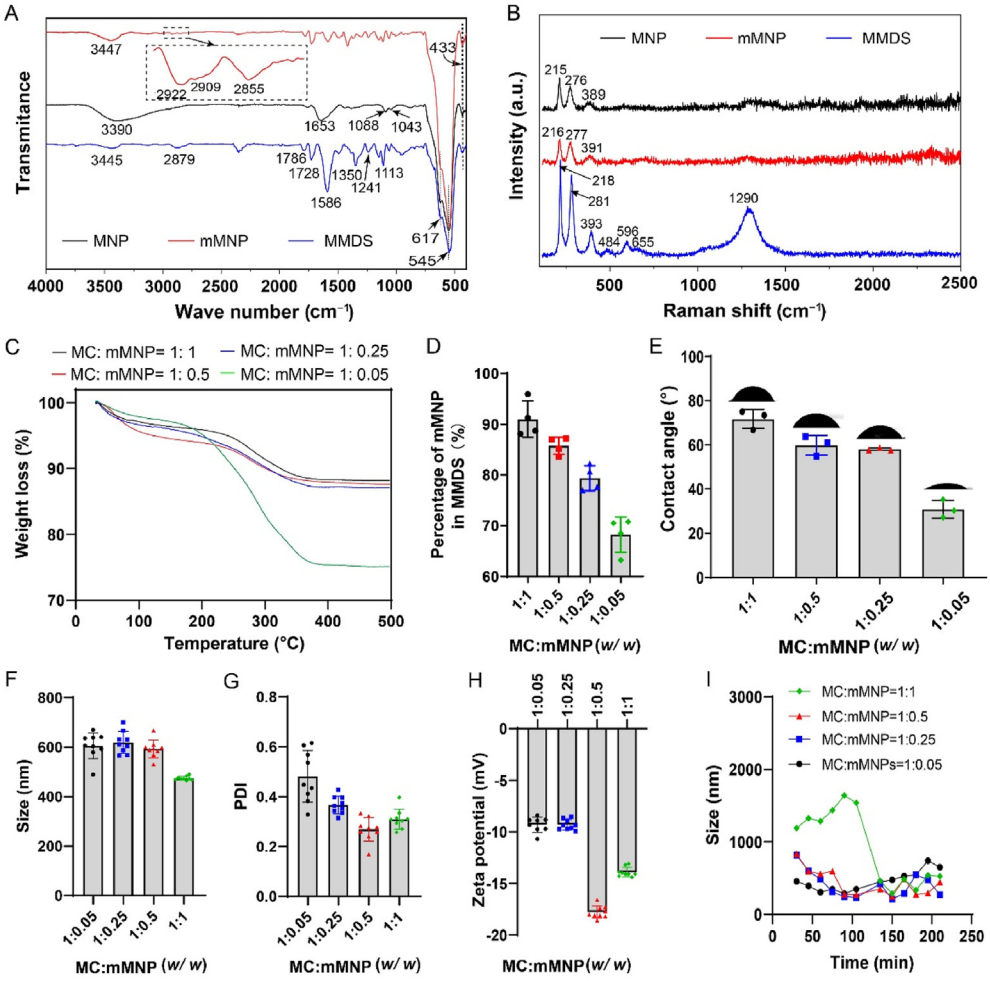

Figure 3 Characterization of the MMDS. (A) FT−IR spectra of the MNP, mMNP, and MMDS. (B) Raman spectra of the MNP, mMNP, and MMDS. (C) TGA diagrams of the MMDS produced by the chemical conjugation of MC and mMNP at varied ratios. (D) The content of MNP in the MMDS (measured by ICP−MS). Data are expressed in mean ± SD ($n = 4$). (E) Changes in the wettability of the MMDS after grafting varied amounts of micelle (MC). Data are expressed in mean ± SD ($n = 3$). (F), (G) and (H) Changes in the size, PDI and zetapotential of the MMDS, respectively, after conjugation of varied amounts of MC. Data are expressed in mean ± SD ($n \geq 5$). (I) Size changes in the MMDS.

(Supporting Information Fig. S9). To visualize the magnetic responsive activity of MMDS, the Nile red was encapsulated into the MC moiety of MMDS (MMDS@NR), and subsequently treated by an external magnet. As shown in Fig. 4E, Supporting Information Video 1 and 2, MMDS@NR can be attracted by an external magnet. As noticed, increasing the amounts of MNPs in the MMDS enhanced their magnetic-responsible effect, thus promoted the recovery of MMDS@NR under the action of magnet (Fig. 4F).

Supplementary video related to this article can be found at https://doi.org/10.1016/j.apsb.2024.05.004

3.3. *MMDS@DEX+MA prolongs DEX-retention in tears while preventing its intraocular transporting*

Tear renewal poses a major non-anatomical barrier for eye surface medication as it can quickly eliminate the drugs from eye surface[16]. The MMDS provided resistance to tear circulation with the assistance of external magnetic field (Fig. 5A). DEX was encapsulated into the MMDS (MMDS@DEX) by hydrophobic interaction, achieving 2%−3% of the encapsulation rate (Fig. 5B). The encapsulation rates were lower than other similar self-assembly systems (usually 5%−10%)[16,24,31,41]. The ratio of MC moiety (serving as DEX carriers) in the MMDS was around 45%, which could explain its low DEX-loading capacity. The released profiles of DEX from the MMDS and MC were investigated. As shown in Fig. 5C, both MMDS and MC could accelerate DEX-diffusion out from dialysis bag to dialysate, when compared to DEX suspension. The pH value of tears ranges from 6.8 to 8.2, which is mainly affected by age, time of day, eye closure, as well as prolonged eye opening[42]. The DEX-release from the MMDS under different pH conditions was investigated. As depicted, the DEX was much easier to be released out from the MMDS in neutral or alkaline conditions, when compared with that in acidic conditions. This could facilitate its application in eye surface medication featuring low drug-bioavailability on account of rapid drug-elimination by lachrymal renewal.

The suspension of MMDS@DEX was topically instilled into the conjunctiva sac of the experimental animals. To enhance the retention of MMDS@DEX on eye surface, the eyes of the animals were covered with devices containing a magnet (Fig. 5A).

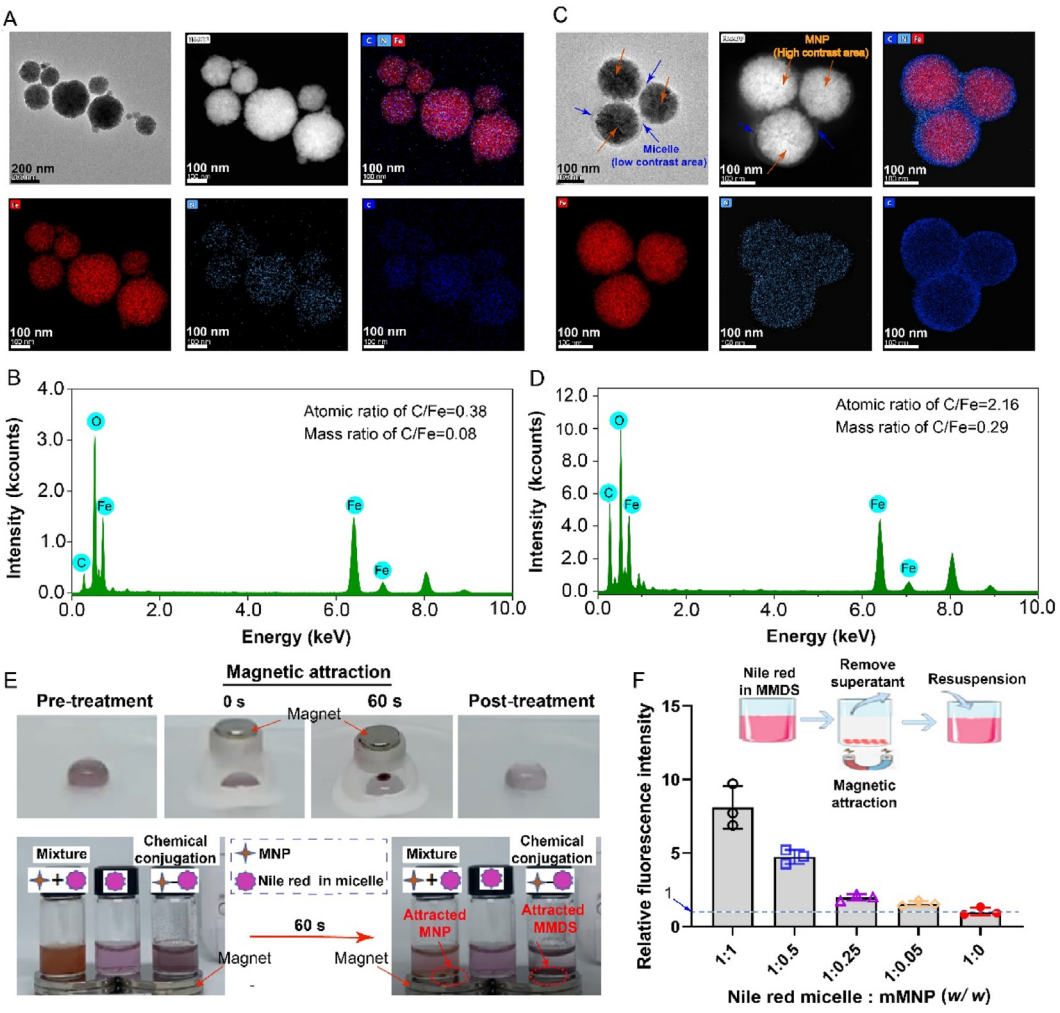

Figure 4 Morphologies and magnetic responsive properties of the MMDS. (A) TEM images and EDS elemental mapping of the MNP. (B) EDS spectra of the MNP. (C) TEM images and EDS elemental mapping of the MMDS. The micelle moiety (low contrast area under TEM) and MNP moiety (high contrast area under TEM) in the MMDS were indicated by blue and orange arrows, respectively. (D) EDS spectra of MMDS. (E) Magnetic effects of MMDS@NR. (F) The recovery of MMDS@NR after magnetic decantation. Data are expressed in mean ± SD (n = 3).

After administrating MMDS@DEX+MA, DEX reached 286.7 ng in each sampling medium (waterman No.1 filter paper) at first 5 min after instillation, compared to a content of 202.2 ng by MMDS@DEX treatment (without magnetic attraction) (Fig. 5D). The concentration of DEX in tears remarkably dropped 77.3 ng for MMDS@DEX+MA and 41.9 ng for MMDS@DEX treatments in 15 min after instillation (Fig. 5D), probably due to the rapid tear renewal which removed the drug from eye surface. Magnetic attraction of MMDS@DEX significantly prolonged the eye surface retention of DEX, significantly higher in the area under curve (AUC) than the non-magnetic attraction counterpart (Supporting Information Fig. S10A), which could enhance its therapy effects to some extent. It is noteworthy that the cornea and conjunctiva are the utmost tissues of eyes in anatomy, and inflammations in corneas and conjunctivas are the most common disorder in eye surface reacting to a variety of stimulus. DEX, one of the corticosteroids molecules, is the most effective for treating this non-specific inflammation[43]. Accumulation efficiency of DEX in corneas and conjunctivas could enhance its therapy effects against these kinds of inflammations. As depicted in Fig. 5E and S10B, magnet treatment dramatically improves the accumulation of MMDS@DEX in corneas by > 10 times than the non-magnet group at 5 min after administration. Higher contents of DEX in corneas with MMDS@DEX+MA treatments are also observed at 2 and 4 h after administration, when compared to the non-magnet treated group. The same trend can also be observed in conjunctivas (Fig. 5F and Fig. S10C). When compared to commercial DEX formulas, MMDS@DEX+MA significantly promoted the DEX retention in tears, corneas, and conjunctivas, while reduced intraocular DEX-transporting (Fig. 5D−G and Fig. S10D). The commercial DEX formula exhibited strong permeability for ocular surface tissues, which resulted in a high DEX content in the aqueous humor. It reached a DEX-concentration of 200 ng/mL in the aqueous humor after 60 min of commercial DEX administration (topical instillation), which was ten times than that of the MMDS@DEX+MA treated group (Fig. 5G). *In vivo* Nile red retention in corneas was observed when MMDS@NR+MA was applied (Supporting Information Fig. S11), which confirmed the effects of the magnet treatment in prolonging drug retention in ocular surface tissues. In addition, limited amount of DEX can be detected in

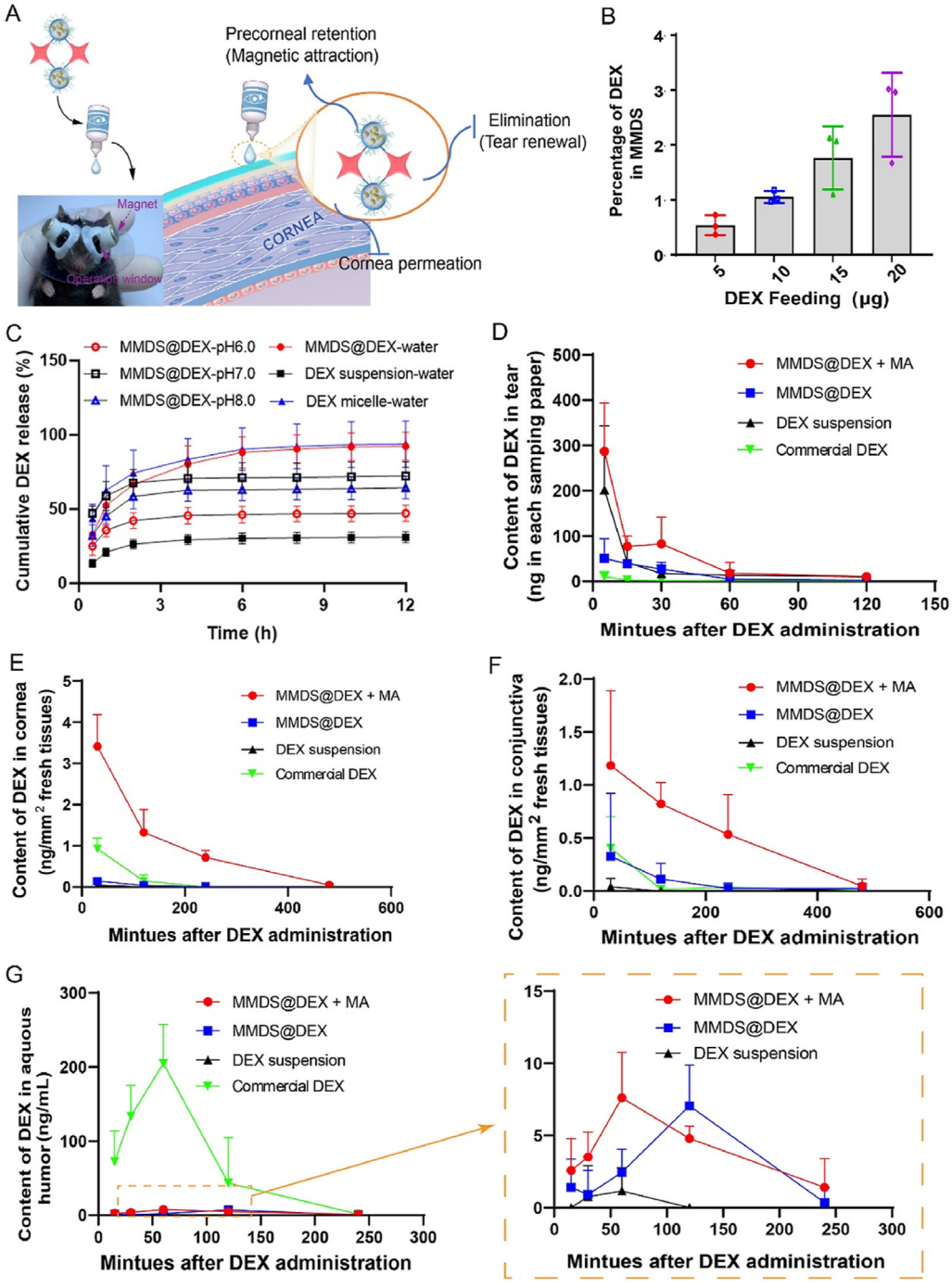

Figure 5 MMDS@DEX with magnetic attraction increased DEX contents in the cornea and conjunctiva while reduced DEX concentration in the aqueous humor. (A) Schematic illustration of utilizing the MMDS for effective DEX delivery in ocular surface application. (B) The DEX-encapsulation capacity of the MMDS. Data are expressed in mean ± SD ($n = 3$). (C) The *in vitro* DEX release profiles. (D)−(G) The *in vivo* time-related DEX contents in tears, corneas, conjunctivas, and the aqueous humor with receiving of varied treatments. The magnetic field was used throughout the experimental time range. Data are expressed in mean ± SD ($n = 5$). (H) The effects of the treatments on the intra-ocular pressure (IOP) of the experimental animals. (I)−(M) The *in vivo* time-related iron retention in the cornea, conjunctiva, lacrimal gland, aqueous humor, and retina of the experimental animals, respectively, after receiving MMDS@DEX instillation with or without combination of MA treatment. The magnetic field was used throughout the experimental time range. Data are expressed in mean ± SD ($n \geq 3$). $^{*}P < 0.05$, $^{**}P < 0.01$, $^{***}P < 0.001$, $^{\#}P < 0.05$, $^{\#\#}P < 0.01$, and $^{\#\#\#}P < 0.001$ vs. shCtrl or indicated. The significance analysis was conducted by one-way ANOVA analysis.

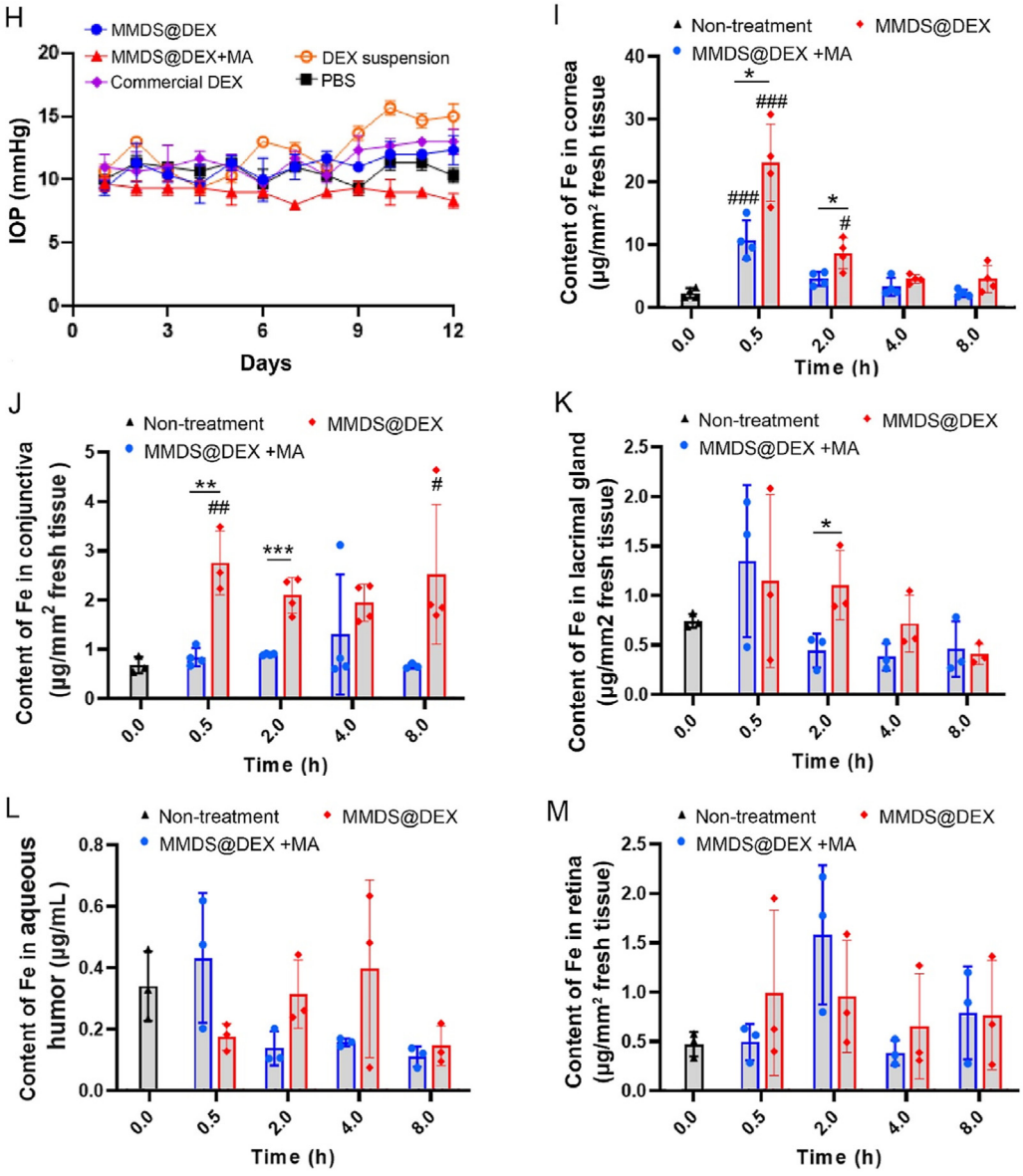

Figure 5 (*continued*)

tears, corneas, and conjunctivas with DEX suspension (Fig. 5D−G and Fig. S10). These results indicate that the combination of topical administration of MMDS@DEX with a magnet treatment could enhance its ability to resist tear renewal and promote DEX accumulation in corneas and conjunctivas.

3.4. *MMDS@DEX+MA avoids DEX induced IOP rising*

Escalation in IOP is the most addressed side effect of the commercial DEX eye drop. In the present study, the effect of continuous instillation of MMDS@DEX with or without magnet treatments on IOP was evaluated in time course. As shown in Fig. 5H and Supporting Information Fig. S12, healthy rats have an IOP around 10 mmHg. Continuous application of DEX suspension and commercial DEX eye drops significantly escalated IOP. Topical administration of MMDS@DEX without magnet treatment elevated IOP by 1.5 times than that of the PBS administrated group in a 12-day continuous treatment at a frequency of 3 times per day. With combination of magnet treatment, continuous expose of MMDS@DEX on eye surface did not significantly promote the IOP level, indicating that this treatment strategy is effective in enhancing the safety of DEX, probably due to that it reduces the intraocular transporting of DEX.

3.5. *MMDS@DEX+MA prevents iron accumulation in ocular tissues*

Iron overload has been intensively investigated to be harmful to the ocular tissues (*e.g.*, cornea, conjunctiva, retina) mainly by ROS production[30,44]. Therefore, to further understand the safety perspective of the present treatment, the iron contents in the cornea, conjunctiva, lacrimal gland, aqueous humor, retina, and lens after topical instillation of MMDS@DEX with and without magnet treatments were compared and studied. As shown in Fig. 5I and J, the application of MMDS@DEX (without magnet treatment) has significantly increased the iron levels both in the conjunctiva and cornea (compared to the untreated group) in the first 2 h of administration. However, combination of magnet

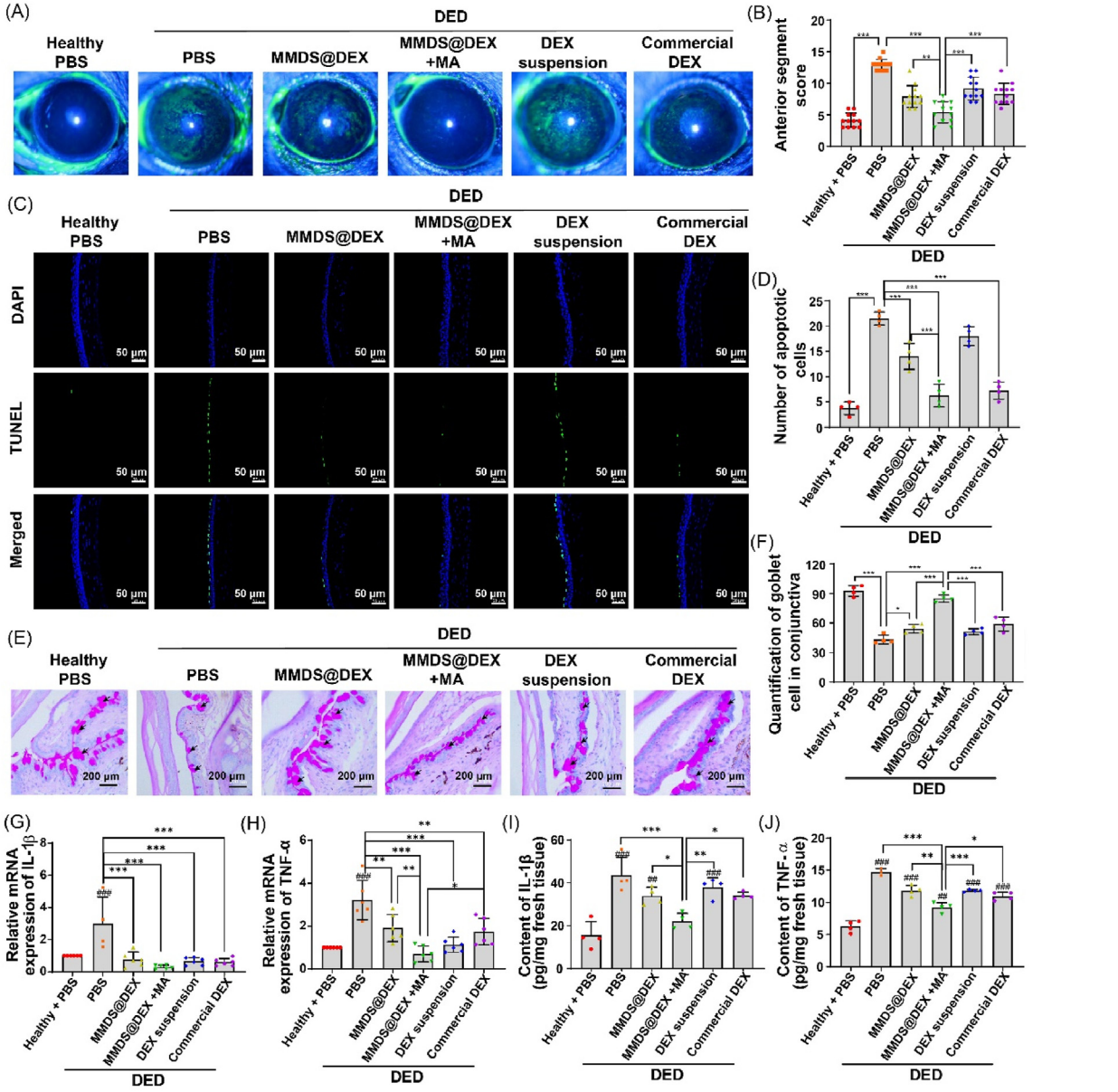

Figure 6 MMDS@DEX with magnetic attraction enhanced the therapy effects against DED. (A) Representative images of corneas receiving varied treatments (recorded under a slit-lamp microscope after fluorescein staining; (B) The score of the cornea of experimental animals. Data are expressed in mean ± SD ($n = 12$). $^{*}P < 0.05$, $^{**}P < 0.01$, $^{***}P < 0.001$ vs. shCtrl or indicated. (C) Representative fluorescence images of corneas after TUNEL staining (scale bar = 50 μm). (D) The quantitative analysis of the TUNEL positive cells in the cornea. Data are expressed in mean ± SD ($n = 4$). $^{*}P < 0.05$, $^{**}P < 0.01$, $^{***}P < 0.001$ vs. shCtrl or indicated. (E) Representative images of conjunctival epithelium after PAS staining. The PAS positive goblet cell is indicated by black arrows (scale bar = 200 μm). (F) Quantitative analysis of the conjunctival goblet cell. Data are expressed in mean ± SD ($n = 4$). $^{*}P < 0.05$, $^{**}P < 0.01$, $^{***}P < 0.001$ vs. shCtrl or indicated. (G) and (H) Relative mRNA expression of IL-1β and TNF-α after receiving varied treatments. (I) and (J) Protein quantification of IL-1β and TNF-α by ELISA assays after receiving varied treatments. Data are expressed in mean ± SD ($n = 4$). $^{*}P < 0.05$, $^{**}P < 0.01$, $^{***}P < 0.001$, $^{\#}P < 0.05$, $^{\#\#}P < 0.01$, and $^{\#\#\#}P < 0.001$ vs. shCtrl or indicated.

treatment for MMDS@DEX instillation did not cause the iron-overloading both in the conjunctiva and cornea. Moreover, MMDS@DEX+MA could also reduce the Fe levels in the lachrymal gland (Fig. 5K), aqueous humor (Fig. 5L), retina (Fig. 5M), and lens (Supporting Information Fig. S13), when compared to the single MMDS@DEX groups. These suggested that magnet treatment could reduce the risk of iron-toxicity of MMDS to ocular tissues.

3.6. MMDS@DEX+MA enhances the in vivo curing effects against DED

To prepare the DED-animal model, scopolamine was intraperitoneally injected into mice. DED-induced animals were evaluated by a skilled doctor according to the generally adopted clinical diagnostic criteria. As shown in Fig. 6A, the healthy animals possessed clear and deep blue corneas when viewed under a slit lamp microscope,

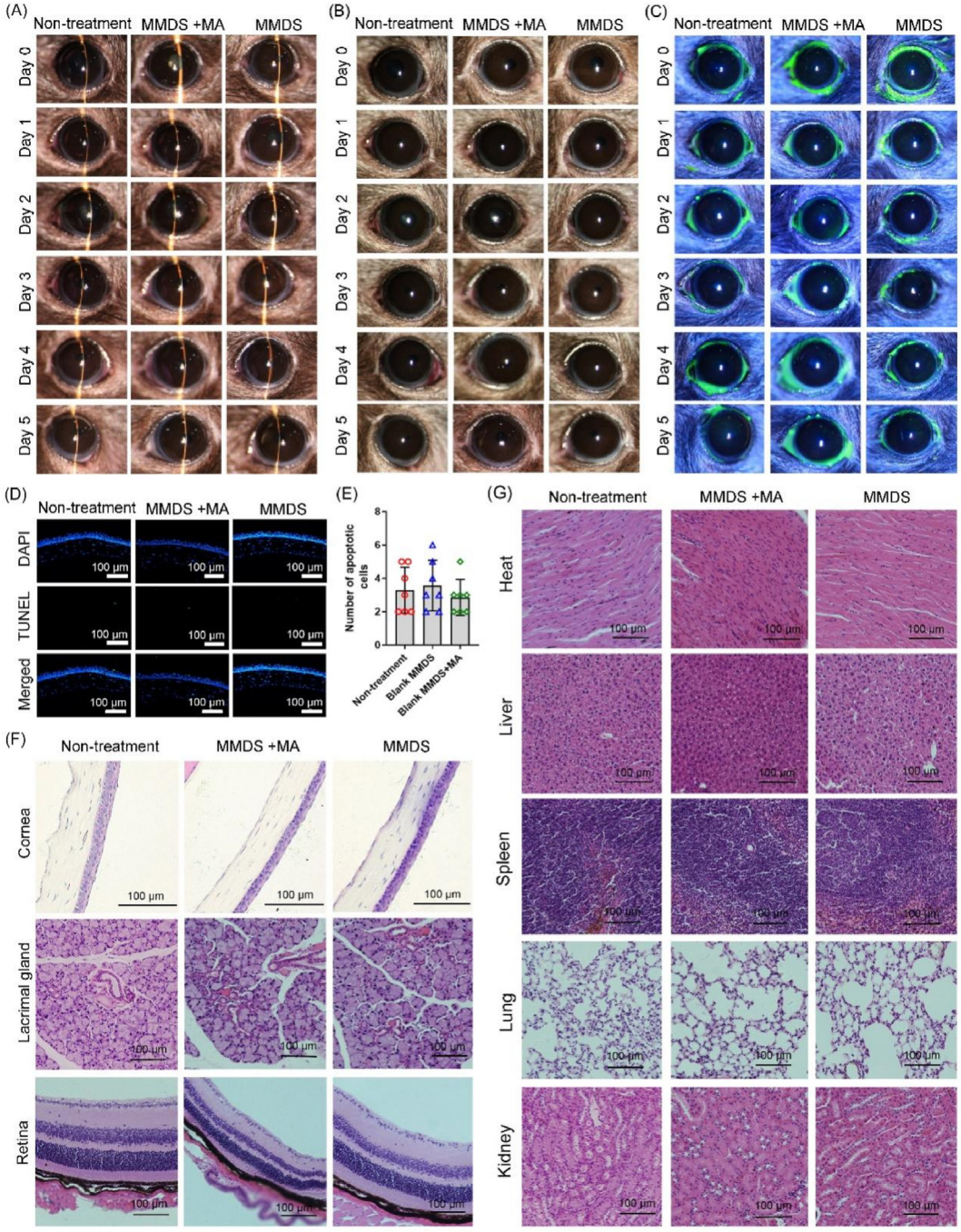

Figure 7 The *in vivo* ocular toxicity of the instilled MMDS suspension with or without external magnet attraction (MA). (A), (B) and (C) Slit lamp observation under narrow slit beam, red-free beam, and cobalt blue beam after fluorescein sodium staining, respectively. (D) Representative images of TUNEL assay (scale bar = 100 μm). (E) Quantification of the apoptotic cells calculated from the TUNEL results (n = 7). (F) and (G) Representative images of H&E staining (scale bar = 100 μm).

which were consistence with previous observation[16,17]. The cornea of the animals receiving scopolamine treatment exhibited a diffused contiguous fluorescence staining, indicating the occurrence of DED. The DEX suspension and the commercial DEX formula presented limited capacity to reduce scopolamine induced DED-symptoms. The combined treatment of MMDS@DEX instillation and magnetic attraction (MMDS@DEX+MA) showed obvious therapeutic effects than the MMDS@DEX counterpart, which apparently alleviated DED-symptoms to a healthy level (Fig. 6B). To further understand the therapy effects, the animals were sacrificed and the eyes were extracted. The tissue sections of corneas and conjunctivas were extracted for further examination. The cornea sections were subjected to TUNEL assays. As shown in Fig. 6C and D, intraperitoneal injection of scopolamine caused substantial apoptosis of corneal epithelium. Topical instillation of MMDS@DEX (without magnetic attraction) exerted significant effects to inhibit corneal epithelium apoptosis; whereas its level of cornea epithelium apoptosis is still significantly higher than that in

the healthy group. It is evident that both the MMDS@DEX+MA and commercial DEX treatments can significantly reduce the level of corneal epithelium apoptosis in the healthy group (no significant reduction in the healthy control).

Since DED also induces the conjunctival goblet cell loss by favoring continuous ocular surface inflammation[45,46]. We further evaluated the protective effects of these DEX formulas against goblet cell apoptosis under DED. As depicted in Fig. 6E and F, intraperitoneal injection of scopolamine remarkably induced conjunctival goblet cell loss, while topical instillation of commercial DEX formula, DEX suspension, and MMDS@DEX exerted moderate cell protective effects. However, the density of goblet cells in commercial DEX formula-, DEX suspension-, and MMDS@DEX-treated groups is significantly lower than that in the healthy group. MMDS@DEX+MA treatment exerted powerful ability to reduce goblet cell apoptosis, which regulated the goblet cell density to the level of the healthy group.

Owing to DED's "vicious circle of inflammation"[45], the expressions of several inflammatory cytokines were evaluated using RT-PCR. As depicted in Fig. 6G and H as well as Supporting Information Fig. S14, intraperitoneal injection of scopolamine caused the mRNA overexpression of IL-1β, TNF-α, IFN-γ, and IL-6 by 2−5 times compared to the un-treated counterpart. All this DEX showed significant capacity to suppress the mRNA overexpression of those inflammatory cytokines. Among these treatments, MMDS@DEX+MA treatment exerted significantly higher mRNA expression of TNF-α than that of MMDS@DEX-, DEX suspension-, and commercial DEX-treatments. Since these treatments exerted similar levels of capability to suppress mRNA expression of IL-1β, IFN-γ, and IL-6, the contents of IL-1β and TNF-α cytokines in ocular surface tissues were further measured by ELISA. As shown in Fig. 6I and J, the MMDS@DEX+MA treatments possessed significantly higher ability to suppress contents of IL-1β and TNF-α in eye surface tissues, consequently providing better therapy effects against DED.

3.7. *The in vitro and in vivo toxicity of MMDS*

The *in vitro* and *in vivo* toxicity of MMDS suspension were evaluated using eye surface cells and tissues. The cytotoxicity of the MNP, mMNP, and MMDS against human corneal epithelial cells (HCEC) were evaluated using a CCK-8 kit (Supporting Information Fig. S15). The MNP showed dose-dependent cytotoxicity against HCEC, inducing more than 70% of cell death at the concentration of 200 μg/mL. Modification with MMA significantly decreased its toxicity to HCEC. The mMNP at the concentration of 600 μg/mL (iron equivalent) caused >30% of the cell death. No significant cell-growth inhibitions were observed at the MMDS concentration of 0−600 μg/mL (iron equivalent). To understand whether the external magnetic field affects the cell uptake for MMDS, the MMDS@NR were co-cultured with HCEC under magnet treatment. The effects of single MMDS@NR treatment were compared. The results suggested that the external magnetic field affected cellular uptake for MMDS@NR in a short-term culturing (3 and 6 h). It did not affect cellular uptake in a long-term culturing (12 and 24 h, Supporting Information Fig. S16). To evaluate the *in vitro* cumulative ocular-toxicity, the MMDS was topically administration 3 times/day continuously for 12 days. The MMDS instillation with and without combination of magnet treatment were compared. As shown in Fig. 7, the application of MMDS with and without magnet treatment did not cause obvious pathological (Fig. 7A−C) and histological (Fig. 7D−F) change in corneas.

4. Conclusions

The present work developed a novel MMDS system by chemical conjugation of MNPs and MC. The MC moiety in the MMDS served as the carrier for hydrophobic molecules and the MNP part endows the MMDS with magnetic responsive properties. After topical instillation of MMDS, the retention of the drugs (in the MMDS) on eye surface was remote-controlled by external magnetic field. The MMDS was applied to load DEX. With combination of magnet treatment, MMDS@DEX exerted significantly higher therapeutic effects against DED than those treatments of DEX suspension, commercial DEX eye drops, and MMDS@DEX without magnet treatment, which is probably due to its increased DEX-bioavailability by using MMDS@DEX+MA. Moreover, administration of MMDS@DEX with magnet attraction exerted higher long-term bio-safety than commercial DEX eye drops and MMDS@DEX without magnet treatment. As continuous instillation of commercial DEX eye drops significantly promote IOP conditions, the present approach did not cause escalation of IOP in a continuous 15-day application time period. This study provided a new method for effective delivery of hydrophobic agents to eye surface tissues, which will benefit for the treatments of a wide range of eye surface diseases.

Acknowledgments

This work was financially supported by National Natural Science Foundation of China (No. 82070932), the Zhejiang Provincial Natural Science Foundation of China (No. LY19H120002), the internal funding of Wenzhou Medical University (No. KYYW202020, China). The Project of Wenzhou Medical University Affiliated Eye Hospital (No. YNZD2201901, China), and the integration project of State Key Laboratory of Ophthalmology, Optometry and Vision Science (No. J02-20190202, China).

Author contributions

Sen Lin, Wei Chen, Jianliang Shen, and Kaihui Nan supervised this work. Qinxiang Zheng, Chaoxiang Ge, Kexin Li, and Xiaoyu Xia carried out the experiments. Sen Lin, Xiao Liu, and Longxin Wang wrote the manuscript. Rashid Mehmood, Kaihui Nan, and Wei Chen proofread the manuscript. Sen Lin, Longxin Wang, and Qinxiang Zheng analyzed a part of the data. All authors have read and approved the final version of the manuscript.

Conflicts of interest

The authors declare no conflicts of interest.

Appendix A. Supporting information

Supporting information to this article can be found online at https://doi.org/10.1016/j.apsb.2024.05.004.

References

1. Craig JP, Nichols KK, Akpek EK, Caffery B, Dua HS, Joo CK, et al. TFOS DEWS II definition and classification report. *Ocul Surf* 2017;**15**:276−83.
2. Stern ME, Schaumburg CS, Pflugfelder SC. Dry eye as a mucosal autoimmune disease. *Int Rev Immunol* 2013;**32**:19−41.
3. Bian F, Xiao Y, Barbosa FL, de Souza RG, Hernandez H, Yu Z, et al. Age-associated antigen-presenting cell alterations promote dry-eye inducing Th1 cells. *Mucosal Immunol* 2019;**12**:897−908.
4. Zhang X, Schaumburg CS, Coursey TG, Siemasko KF, Volpe EA, Gandhi NB, et al. $CD8^+$ cells regulate the T helper-17 response in an experimental murine model of Sjogren syndrome. *Mucosal Immunol* 2014;**7**:417−27.
5. Lou Q, Pan L, Xiang S, Li Y, Jin J, Tan J, et al. Suppression of NLRP3/caspase-1/GSDMD mediated corneal epithelium pyroptosis using melatonin-loaded liposomes to inhibit benzalkonium chloride-induced dry eye disease. *Int J Nanomed* 2023;**18**:2447−63.
6. Huang B, Zhang N, Qiu X, Zeng R, Wang S, Hua M, et al. Mitochondria-targeted SkQ1 nanoparticles for dry eye disease: inhibiting NLRP3 Inflammasome activation by preventing mitochondrial DNA oxidation. *J Control Release* 2024;**365**:1−15.
7. Swanson KV, Deng M, Ting JPY. The NLRP3 inflammasome: molecular activation and regulation to therapeutics. *Nat Rev Immunol* 2019;**19**:477−89.
8. Guan M, Ma H, Fan X, Chen X, Miao M, Wu H. Dexamethasone alleviate allergic airway inflammation in mice by inhibiting the activation of NLRP3 inflammasome. *Int Immunopharmacol* 2020;**78**:106017.
9. Feng X, Zhao Y, Yang T, Song M, Wang C, Yao Y, et al. Glucocorticoid-driven NLRP3 inflammasome activation in hippocampal microglia mediates chronic stress-induced depressive-like behaviors. *Front Mol Neurosci* 2019;**12**:210.
10. Zhang X, Wang Z, Zheng Y, Yu Q, Zeng M, Bai L, et al. Inhibitors of the NLRP3 inflammasome pathway as promising therapeutic candidates for inflammatory diseases (Review). *Int J Mol Med* 2023;**51**:35.
11. Smits HH, Grünberg K, Derijk RH, Sterk PJ, Hiemstra PS. Cytokine release and its modulation by dexamethasone in whole blood following exercise. *Clin Exp Immunol* 1998;**111**:463−8.
12. Taube M, Carlsten H. Action of dexamethasone in the suppression of delayed-type hypersensitivity in reconstituted SCID mice. *Inflamm Res* 2000;**49**:548−52.
13. Dhabhar FS, McEwen BS. Enhancing versus suppressive effects of stress hormones on skin immune function. *Proc Natl Acad Sci USA* 1999;**96**:1059−64.
14. Patel GC, Phan TN, Maddineni P, Kasetti RB, Millar JC, Clark AF, et al. Dexamethasone-induced ocular hypertension in mice: effects of myocilin and route of administration. *Am J Pathol* 2017;**187**:713−23.
15. Fung AT, Tran T, Lim LL, Samarawickrama C, Arnold J, Gillies M, et al. Local delivery of corticosteroids in clinical ophthalmology: a review. *Clin Exp Ophthalmol* 2020;**48**:366−401.
16. Lin S, Ge C, Wang D, Xie Q, Wu B, Wang J, et al. Overcoming the anatomical and physiological barriers in topical eye surface medication using a peptide-decorated polymeric micelle. *ACS Appl Mater Interfaces* 2019;**11**:39603−12.
17. Zheng Q, Li L, Liu M, Huang B, Zhang N, Mehmood R, et al. In situ scavenging of mitochondrial ROS by anti-oxidative MitoQ/hyaluronic acid nanoparticles for environment-induced dry eye disease therapy. *Chem Eng J* 2020;**398**:125621.
18. Blizzard C, Desai A, Driscoll A. Pharmacokinetic studies of sustained-release depot of dexamethasone in beagle dogs. *J Ocul Pharmacol Th* 2016;**32**:595−600.
19. Chang-Lin JE, Burke JA, Peng Q, Lin T, Orilla WC, Ghosn CR, et al. Pharmacokinetics of a sustained-release dexamethasone intravitreal implant in vitrectomized and nonvitrectomized eyes. *Invest Opth Vis Sci* 2011;**52**:4605−9.
20. Gong Z, Chen M, Wang YW, Huang BS, Chen YJ, Nan KH, et al. Anchoring polyethylene glycol to the ocular surface by phenylboronic acid functionalization: implications for fabrication of long-acting artificial tears. *Colloid Interfac Sci* 2021;**42**:100429.
21. Pranav P, Hitesh P, Shital P, Tejal M. Formulation strategies for drug delivery of tacrolimus: an overview. *Int J Pharm Invest* 2013;**2**:169−75.
22. Battaglia L, Serpe L, Foglietta F, Muntoni E, Gallarate M, Del Pozo Rodriguez A, et al. Application of lipid nanoparticles to ocular drug delivery. *Expert Opin Drug Deliv* 2016;**13**:1743−57.
23. Wang TZ, Guan B, Liu XX, Ke LN, Wang JJ, Nan KH. A topical fluorometholone nanoformulation fabricated under aqueous condition for the treatment of dry eye. *Colloid Surface B* 2022;**212**:112351.
24. Wang D, Huang B, Zhu C, Wang L, Jin J, Tan J, et al. Efficiency encapsulation of FK506 with new dual self-assembly multi-hydrophobic-core nanoparticles for preventing keratoplasty rejection. *Adv Healthc Mater* 2023;**12**:e2203242.
25. Yu A, Shi H, Liu H, Bao Z, Dai M, Lin D, et al. Mucoadhesive dexamethasone-glycol chitosan nanoparticles for ophthalmic drug delivery. *Int J Pharmaceut* 2020;**575**:118943.
26. Tanito M, Hara K, Takai Y, Matsuoka Y, Nishimura N, Jansook P, et al. Topical dexamethasone-cyclodextrin microparticle eye drops for diabetic macular edema. *Invest Ophthalmol Vis Sci* 2011;**52**:7944−8.
27. Bui TQ, Ton SNC, Duong AT, Tran HT. Size-dependent magnetic responsiveness of magnetite nanoparticles synthesised by co-precipitation and solvothermal methods. *J Sci Adv Mater Dev* 2018;**3**:107−12.
28. Wu W, He Q, Jiang C. Magnetic iron oxide nanoparticles: synthesis and surface functionalization strategies. *Nanoscale Res Lett* 2008;**3**:397−415.
29. Walter A, Garofalo A, Parat A, Martinez H, Felder-Flesch D, Begin-Colin S. Functionalization strategies and dendronization of iron oxide nanoparticles. *Nanotechnol Rev* 2015;**4**:581−93.
30. Loh A, Hadziahmetovic M, Dunaief JL. Iron homeostasis and eye disease. *Biochim Biophys Acta* 2009;**1790**:637−49.
31. Wang D, Luo M, Huang B, Gao W, Jiang Y, Li Q, et al. Localized co-delivery of CNTF and FK506 using a thermosensitive hydrogel for retina ganglion cells protection after traumatic optic nerve injury. *Drug Deliv* 2020;**27**:556−64.
32. Su NR, Lv P, Li M, Zhang X, Li M, Niu J. Fabrication of $MgFe_2O_4$−ZnO heterojunction photocatalysts for application of organic pollutants. *Mater Lett* 2014;**122**:201−4.
33. Reddy S, Kumara Swamy BE, Chandra U, Mahathesha KR, Sathisha TV, Jayadevappa H. Synthesis of $MgFe_2O_4$ nanoparticles and $MgFe_2O_4$ nanoparticles/CPE for electrochemical investigation of dopamine. *Anal Methods UK* 2011;**3**:2792−6.
34. Wang JC, Ren J, Yao HC, Zhang L, Wang JS, Zang SQ, et al. Synergistic photocatalysis of Cr(VI) reduction and 4-chlorophenol degradation over hydroxylated alpha-Fe_2O_3 under visible light irradiation. *J Hazard Mater* 2016;**311**:11−9.
35. Demessie AA, Park Y, Singh P, Moses AS, Korzun T, Sabei FY, et al. An advanced thermal decomposition method to produce magnetic nanoparticles with ultrahigh heating efficiency for systemic magnetic hyperthermia. *Small Meth* 2022;**6**:2200916.
36. Yamashita T, Hayes P. Analysis of XPS spectra of Fe^{2+} and Fe^{3+} ions in oxide materials. *Appl Surf Sci* 2008;**254**:2441−9.
37. Idriss H. On the wrong assignment of the XPS O1s signal at 531−532 eV attributed to oxygen vacancies in photo- and electro-catalysts for water splitting and other materials applications. *Surf Sci* 2021;**712**:121894.
38. Ardizzone S, Bianchi CL, Fadoni M, Vercelli B. Magnesium salts and oxide: an XPS overview. *Appl Surf Sci* 1997;**119**:253−9.
39. Sobhanardakani S, Jafari A, Zandipak R, Meidanchi A. Removal of heavy metal (Hg(II) and Cr(VI)) ions from aqueous solutions using Fe_2O_3@SiO_2 thin films as a novel adsorbent. *Process Saf Environ* 2018;**120**:348−57.

40. Lin Z, He M, Liu Y, Meng M, Cao Z, Huang S, et al. Effect of calcination temperature on the structural and formaldehyde removal activity of Mn/Fe_2O_3 catalysts. *Res Chem Intermediat* 2021;**47**:3245−61.
41. Li K, Li R, Zou P, Li L, Wang H, Kong D, et al. Glycopeptide-nanotransforrs eyedrops with enhanced permeability and retention for preventing fundus neovascularization. *Biomaterials* 2022;**281**:121361.
42. Willcox MDP, Argüeso P, Georgiev GA, Holopainen JM, Laurie GW, Millar TJ, et al. TFOS DEWS II tear film report. *Ocul Surf* 2017;**15**:366−403.
43. Leibowitz HM. Management of inflammation in the cornea and conjunctiva. *Ophthalmology* 1980;**87**:753−8.
44. Bellsmith KN, Dunaief JL, Yang P, Pennesi ME, Davis E, Hofkamp H, et al. Bull's eye maculopathy associated with hereditary hemochromatosis. *Am J Ophthalmol Case Rep* 2020;**18**:100674.
45. Bron AJ, de Paiva CS, Chauhan SK, Bonini S, Gabison EE, Jain S, et al. TFOS DEWS II pathophysiology report. *Ocul Surf* 2017;**15**:438−510.
46. Swamynathan SK, Wells A. Conjunctival goblet cells: ocular surface functions, disorders that affect them, and the potential for their regeneration. *Ocul Surf* 2020;**18**:19−26.